Focused polarization ellipse field singularities: interaction of spin-orbital angular momentum and the formation of optical Möbius strips

Physica Scripta

PAPER

Focused polarization ellipse field singularities: interaction of spin-orbital angular momentum and the formation of optical Möbius strips

Sushanta Kumar Pal[1], **Lavi Somers**[1], **Rakesh Kumar Singh**[2], **P Senthilkumaran**[3] and **Ady Arie**[1]

[1] School of Electrical Engineering, Fleischman Faculty of Engineering, Tel Aviv University, Tel Aviv 69978, Israel
[2] Laboratory of Information Photonics and Optical Metrology, Department of Physics, Indian Institute of Technology (Banaras Hindu University), Varanasi, 221005 Uttar Pradesh, India
[3] Optics and Photonics Centre, Indian Institute of Technology Delhi, Hauz Khas, New Delhi 110016, India

E-mail: sushanta1985@gmail.com

Keywords: polarization singularity, optical Mobius strips, tight focusing, ellipse field singularities

OPEN ACCESS

RECEIVED
26 November 2022

REVISED
6 March 2023

ACCEPTED FOR PUBLICATION
29 March 2023

PUBLISHED
6 April 2023

Abstract

We study here the intensity distribution and formation of optical polarization Möbius strips by tightly focusing of C-point singularity beams. These beams are characterized by a central circular polarization point (C-point) surrounded by a spatially varying elliptic polarization. Under tight focusing conditions, the different polarization components of the beam interfere and exhibit clear difference between left-handed and right handed input beams. The transverse polarization distribution at the focal plane is similar to the input distribution for left-handed lemon beam, but exhibits 180° rotation for right handed lemon beam. Moreover, the longitudinal polarization component exhibits spiral phase distribution, owing to spin-orbit angular momentum conversion at the focal plane, with opposite winding directions for the left-handed and right-handed input beams. We show that the shape of the resulting Möbius strip is determined by the helicity of the C-point and by the polarization singularity index, which is the contour integral of polarization ellipse angle around the singularity. It is found that inverting the helicity leads to 180° rotation in the focal plane intensity distribution, accompanied by handedness inversion for the polarization ellipses. The number of separatrices in the input polarization distribution is equivalent to the number of twist points of the Möbius strip in the focal plane, as well as to the number of intensity zeros in the z-component of the focused field. These phenomena are observed for beams with a bright C-point, but also for dark C-point, in which the electric field is zero at the center of the beam.

1. Introduction

The polarization degree of freedom is a useful tool for controlling the properties of light beams. Usually, the polarization is assumed to be nearly uniform in the transverse plane, but in recent years, there was an increasing number of applications that utilized the variation of polarization vector across the transverse plane of the light beam. This enabled to achieve sharper focusing with respect to linearly polarized light [1–4], and to generate significant longitudinal polarization component [2, 4], 3D-polarization structures and singularities [5, 6]. The longitudinal field components enable the formation of complex 3d polarization topologies as optical cones, twisted ribbons and Möbius strips, as predicted by I Freund in 2005 [7] and experimentally demonstrated by T Bauer *et al* in 2015 [8, 9]. Generally, these topologies appear around generic ellipse field singularities, namely, C-points (points of pure circular polarization) and L-points (points of pure linear polarization), in which the orientation or handedness of polarization ellipse is undefined, respectively. First simple but yet striking examples of three-dimensional polarization topologies have been demonstrated recently [8–18], not only by tight focusing but also off-axis interference of two specially synthesized structured beams [10], scattering from high-index dielectric nanoparticles [12], and by the application of all-dielectric metasurfaces [14]. The three-

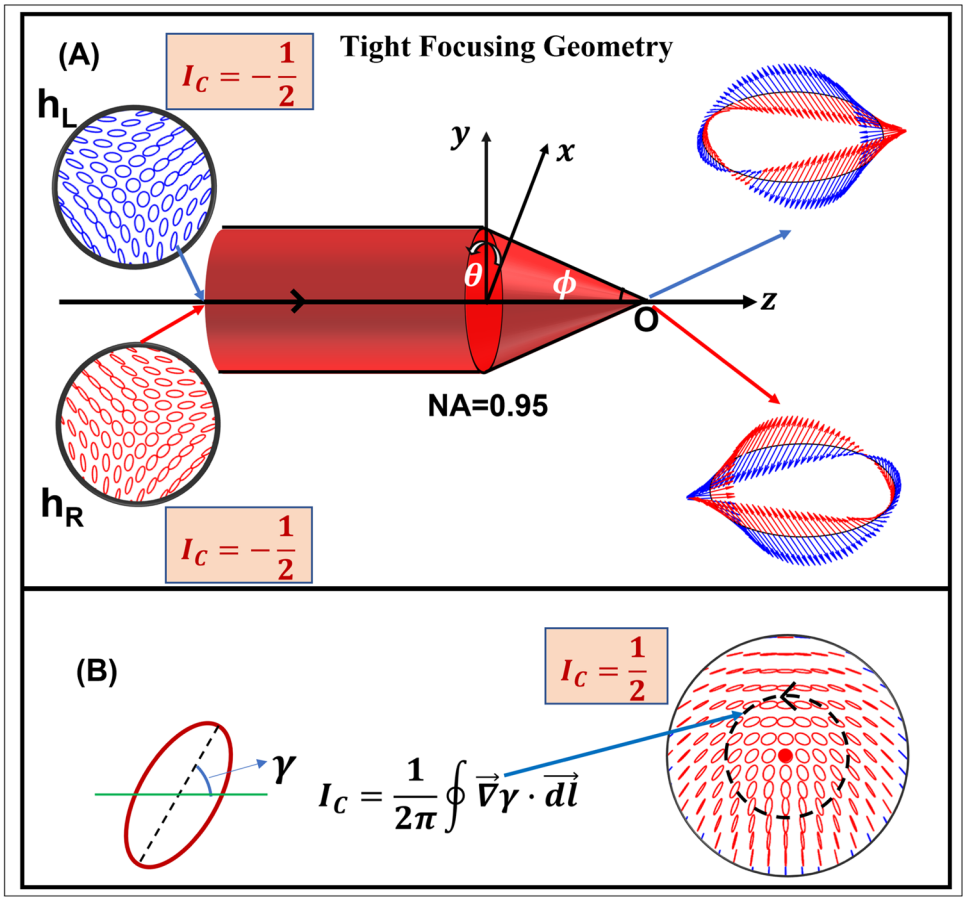

Figure 1. (A)The example shows left and right-handed stars and the corresponding optical Möbius strips at the focal plane. (B) The orientation angle (γ) and the C-point index (I_C) for a polarization ellipse and a lemon distribution are shown.

dimensional structured fields show interesting topological structures such as polarization Möbius strip [7–11, 19–25]. Since it was first proposed, a lot of effort has gone into investigating the polarization Möbius strip [8, 9, 11, 24] and realizing the similar topological structures in various other types of waves [26, 27]. Various topological features of optical Möbius strips are recently investigated [19–23, 25, 28], for example the dependence of polarization Möbius strip on the closed trajectory around the singular point [11, 22, 25]. It is shown that a polarization Möbius strip can become a Möbius-like topology due to a point with photonic wheel [9]. An interesting experiment with Möbius strip microlasers, fabricated with high optical quality by direct laser writing, were studied recently [29].

In this paper, we concentrate on a specific class of beams that contain circular polarization singularities, surrounded by elliptic polarization with continuously varying azimuthal angles. Obviously, at the singularity point, owing to its circular polarization, the azimuthal angle (γ) of the polarization ellipse is not defined. These beams are characterized by the singularity index, I_C [30–32] which is contour integral $\frac{1}{2\pi}\oint \nabla\gamma \cdot dl$ around the singularity, and can acquire only integer or half-integer values. The state of polarization (SOP) distribution for the C-point consists of ellipses and therefore the C-point is also characterized by its helicity, being either left-circular or right-circular [33]. These singular beams can be formed by a superposition of vortex beams with right and left circular polarization, leading to a dark singularity point. In the special case in which one of these two beams is a non-vortex plane wave beam, the singularity point becomes bright. It is interesting to note that the studies that were made so far [8, 13] concentrated only on the latter case of bright singular points. Some of the recently reported applications of polarization singularities are in optical signal processing [34], optical chirality measurements [35], optical trapping and manipulation [36], optical lattices [37, 38], material machining [39], optical skyrmions [40] and structured illumination microscopy [41].

The unique properties of the circular polarization singularities become dominant when the beam is tightly focused, so that different polarization components are mixed, which also leads to the creation of a longitudinal polarization component, in addition to the two transverse components. Recently, polarization singularities with V-points [42, 43] (i.e. vector beams with undefined linear polarization at the singular points) and C-points [8, 13, 44] have been used to shape the focal spot intensity distribution. Owing to the emerging interest and vast

applications of these beams, there is a need for a complete study on the effects of helicity and singularity index, for both the bright and the dark singularities, and to compute the intensity, phase distribution and optical Möbius strips at the focal plane in these cases. Specifically, we compare beams that have the same C-point singular index, but opposite helicity [45, 46]. This comparison is made for three different values of the singularity index.

2. Ellipse field singularities and tight focusing

Polarization singularities (C-points and V-points) are generally identified by using the complex field known as Stokes field $S_{12}(x, y) = S_1(x, y) + iS_2(x, y) = |S_{12}(x, y)| \exp(i\phi_{12}(x, y))$. The Stokes phase is $\phi_{12}(x, y) = 2\gamma(x, y)$ and it can be shown that it is the phase difference between left and right -handed components in the circular basis, i.e., $\phi_{12}(x, y) = \phi_L(x, y) - \phi_R(x, y)$. Therefore, phase vortices of S_{12} Stokes field are polarization singularities (C-points and V-points). The expression of ellipse field singularities in paraxial optical fields, under circular polarization basis decomposition [8, 30, 47], can be given by,

$$\vec{E}(r, \theta) = \Psi_L \hat{e}_L + \Psi_R \hat{e}_R = B_1 r^{|m|} e^{im\theta} \hat{e}_L + B_2 r^{|n|} e^{i(n\theta+\theta_0)} \hat{e}_R, \tag{1}$$

where $\hat{e}_L$ and $\hat{e}_R$ are left and right circular unit basis vectors respectively. In equation (1), the integers m, n are the topological charges of the phase vortex beams with amplitude scaling factors B_1 and B_2 respectively, θ is azimuthal angle and θ_0 is initial phase shift given to one of the beams. For a bright C-point either m or n is zero and $|m| \neq |n|$. So far, most studies concentrated on this type of beam [30, 32]. However, as noted above, there is also another case, where $|m| \neq |n|$, and both indices are non-zero, that results in a non-generic dark C-point [48–50]. Since $|m|$ and $|n|$ are non-zero, the component vortex beams forming the C-point singularities themselves as well as the resultant field have intensity nulls at the singular point. The handedness of the dark C-point is therefore taken as a limiting case of the handedness as we approach the singularity in the radial direction [48]. The superposition described by equation (1) can be realized by the Mach–Zehnder type interferometer, where the two arms carry the right circular and left circularly polarized beams, respectively. For the field given by equation (1), the C-point index (I_C) is $I_C = (n - m)/2$, where $|m| \neq |n|$.

Let us now consider what happens when these beams are focused by a lens with a numerical aperture (NA), given by $NA = n_0 \sin \phi_{\max}$, where n_0 is the refractive index of the focal region and $\phi_{\max}$ is the maximum angle of convergence. For an optical system shown in figure 1(A), the electric field components in the focal region of an aberration-free aplanatic lens are given by [51, 52]

$$E(u, v) = (-iA/\lambda) \int_0^{\phi_{\max}} \int_0^{2\pi} E_2(\phi) P(\phi, \theta) A_2(\phi) e^{\left(-i\frac{v}{\sin\phi_{\max}} \sin\phi \cos(\theta-\theta_P)\right)} \times e^{\left(-i\frac{u}{\sin^2\phi_{\max}} \cos\phi\right)} \sin\theta d\phi d\theta. \tag{2}$$

where A is linked to the optical system parameters and λ is the wavelength of light in the medium with refractive index (n_0) in the focal region and ϕ is the focusing angle. $E_2(\phi)$ is given by

$$E_0 e^{-\Gamma^2\rho^2} = E_0 e^{(-\Gamma^2 \sin^2\phi/\sin^2\phi_{\max})} = E_2(\phi), \tag{3}$$

where E_0 is the amplitude of the beam, $\rho = \sin\phi/\sin\phi_{\max}$ is the radial distance of a point from the center, normalized by the radius (a) of the lens. The truncation parameter is given by $\Gamma = a/w$, where w is the beam waist. It is a measure of the fraction of the beam inside the physical aperture of the lens. $P(\phi, \theta)$ denotes polarization distribution at the exit pupil and $A_2(\phi)$ is the apodization factor. For an aplanatic lens system $A_2(\phi)$ is $\sqrt{cos\phi}$. The polarization distribution ($P(\phi, \theta)$) of the input field at the exit pupil can be expressed as

$$\begin{pmatrix} a_1(\cos\phi\cos^2\theta + \sin^2\theta) + b_1(\cos\phi\sin\theta\cos\theta - \sin\theta\cos\theta) \\ a_1(\cos\phi\sin\theta\cos\theta - \sin\theta\cos\theta) + b_1(\cos\phi\sin^2\theta + \cos^2\theta) \\ -a_1\sin\phi\cos\theta - b_1\sin\phi\sin\theta \end{pmatrix}, \tag{4}$$

where $a_1(r, \theta) = (r^{|m|}e^{im\theta} + r^{|n|}e^{in\theta})$ and $b_1(r, \theta) = i(r^{|m|}e^{im\theta} - r^{|n|}e^{in\theta})$ are the strengths of the x and y components of the input field respectively.

3. Spin-orbit angular momentum coupling and inversion of transverse polarization distribution in C-point singularities

The optical angular momentum of photons is one of the fundamental properties of the electric field. In a seminal paper by Zhao *et al* [53] it is shown that optical spin to orbital angular momentum conversion can occur in a homogeneous and isotropic medium. Photons have two different types of angular momenta, namely spin angular momentum (SAM), with angular momentum $\hbar\sigma$ ($\sigma = +/-1$ for left/right circular polarization) and

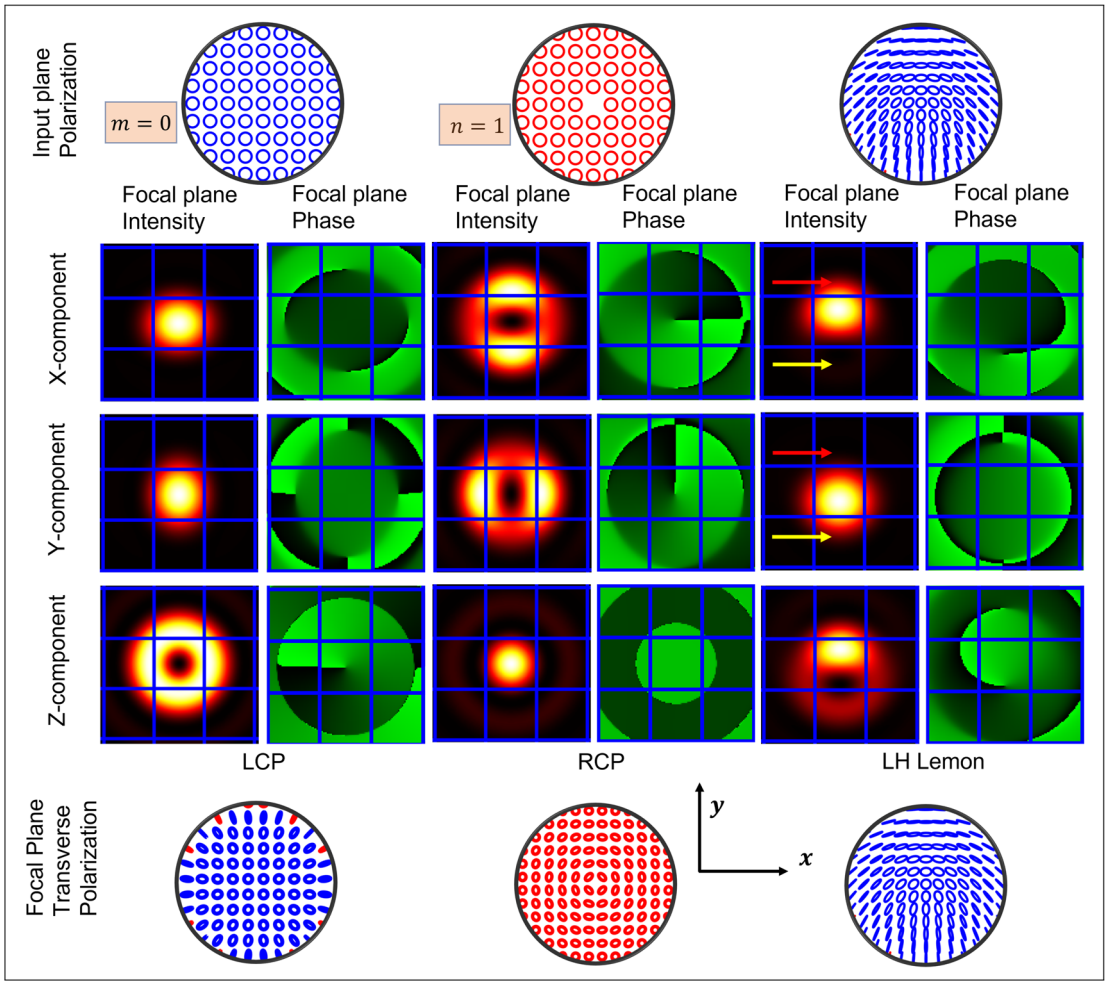

Figure 2. Spin to orbital angular momentum conversion in left-handed lemon. Input plane polarization distributions are shown in row I. Focal plane intensity and phase corresponding to *x*, *y*, and *z*-components are shown in row II, row III, and row IV respectively. Focal plane transverse polarization distributions are shown in the bottom row.

Table 1. Parameters of ellipse field singularity beams. The C point index is $I_C = (n - m)/2$. For all cases, the number of half twists is $(|2I_C - 2|)$. The direction of rotation is clockwise (counter-clockwise) for negative (positive) value of $(2I_C - 2)$.

Figure	I_C	(m, n)	Direction of rotation	No. of half-twists
4(a)	$\frac{1}{2}$	$(0, 1)$	Clockwise	1
4(b)	$\frac{1}{2}$	$(-1, 0)$	Clockwise	1
4(c)	$\frac{-1}{2}$	$(0, -1)$	Clockwise	3
4(d)	$\frac{-1}{2}$	$(1, 0)$	Clockwise	3
4(e)	$\frac{3}{2}$	$(0, 3)$	Counter-clockwise	1
4(f)	$\frac{3}{2}$	$(-3, 0)$	Counter-clockwise	1
4(g)	$\frac{-3}{2}$	$(0, -3)$	Clockwise	5
4(h)	$\frac{-3}{2}$	$(3, 0)$	Clockwise	5
4(i)	$\frac{1}{2}$	$(1, 2)$	Clockwise	1
4(j)	$\frac{1}{2}$	$(-2, -1)$	Clockwise	1

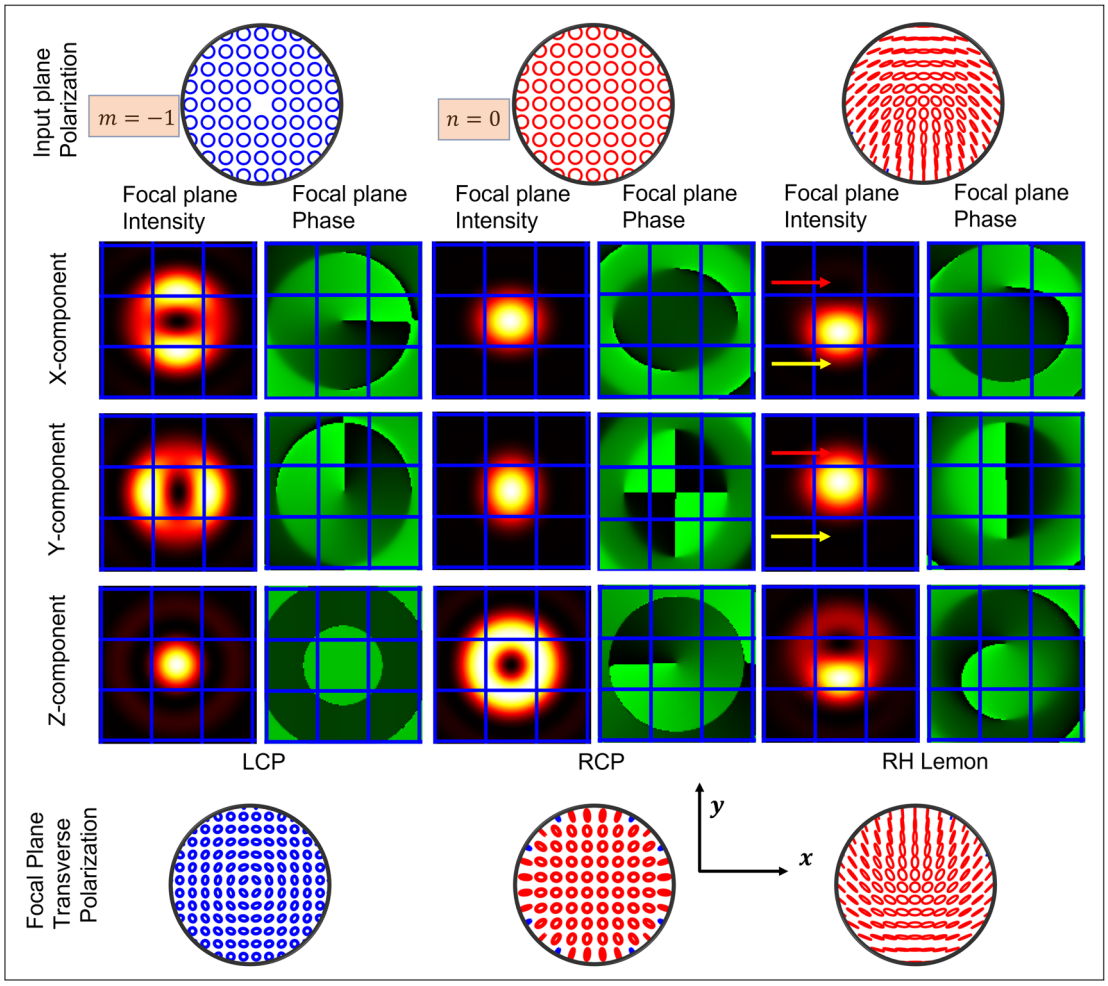

Figure 3. Spin to orbital angular momentum conversion in right-handed lemon. Input plane polarization distributions are shown in row I. Focal plane intensity and phase corresponding to *x*, *y*, and *z*-components are shown in row II, row III, and row IV respectively. Focal plane transverse polarization distributions are shown in the bottom row.

orbital angular momentum (OAM), with angular momentum $l\hbar$, where l is an integer number. The SAM is associated with circular polarization, whereas OAM is linked to the helical phase of light respectively. In the case of a trapped particle, the spinning of a particle around its own axis is due to SAM, whereas the orbiting of the particle around the beam axis is due to OAM of the optical field [54, 55]. The evidence of inter-transfer of spin-to-orbital angular momentum is shown by tight focusing left and right circularly polarized vortex beams. It was shown that the phase of the longitudinal component of a focused beam contains the term $e^{i(l\pm1)\theta}$, where θ is the azimuthal angle [56].

Whereas the input beams that were considered so far in [54, 55] had homogeneous transverse polarization (i.e. having either right of left circular polarization over the entire transverse plane) in this article, we consider input beams with spatially varying polarization [57]. We show that also in this case of tight focusing of left and right-handed C-point polarization singularities, the spin–orbit coupling plays an important role. In order to understand it, we shall examine the focusing properties of left-handed and right-handed lemon beams. A left-handed lemon is realized by combining a left-handed circularly polarized light($m = 0$) with a right-handed circularly polarized vortex beam($n = 1$), whereas a right-handed lemon is realized by combining a right-handed circularly polarized light($n = 0$) with a left-handed circularly polarized vortex beam($m = -1$). Figure 2 shows the component intensity and phase distributions of a left-handed lemon at the focal plane of a high numerical aperture lens. The longitudinal component is shown in the fourth row, where for the left circularly polarized light, the transfer of spin-to-orbital angular momentum is manifested by an helical phase front at the focal plane, whereas for the right circularly polarized vortex beam, the phase contributions of the spin and orbital angular momenta cancel each other and the phase becomes nearly constant at the central region. The focal plane distribution of the focused left-handed lemon is obtained by combining these two fields, which leads to the spiral winding phase. This is a manifestation of spin–orbit coupling for a beam with structured polarization profile.

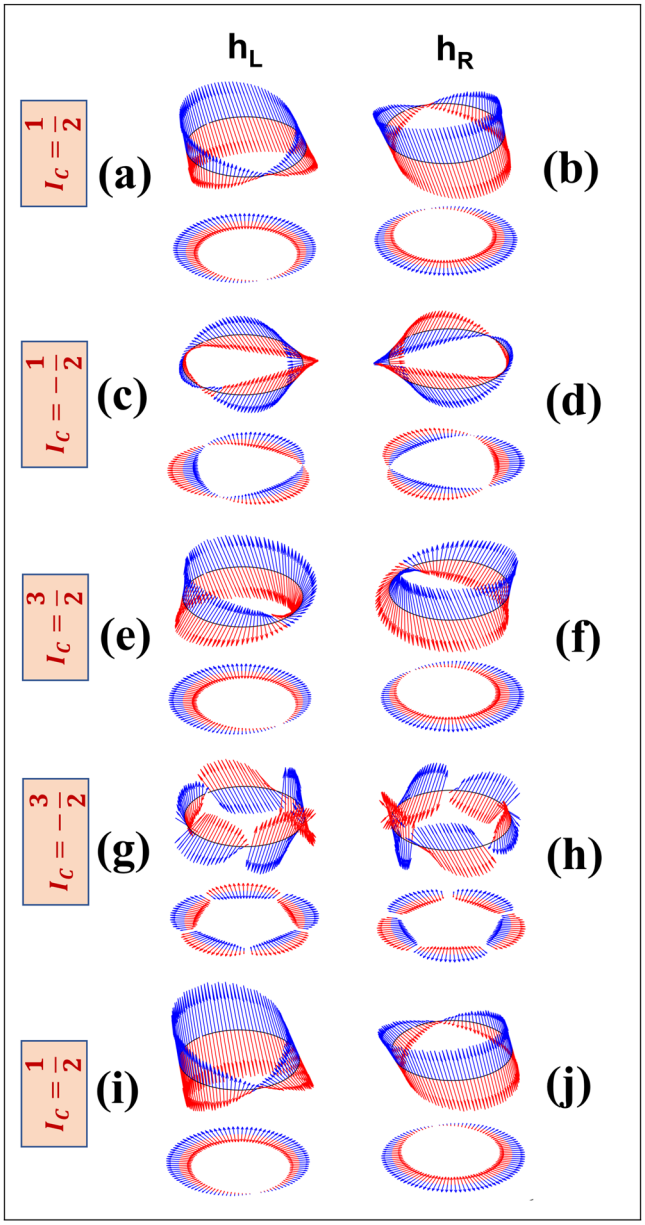

Figure 4. Three-dimensional polarization topology of non-paraxial ellipse field singularities. The numerically calculated polarization topology in the focal plane of (a)–(b) $I_C = \frac{1}{2}$; (c-d) $I_C = \frac{-1}{2}$; (e-f) $I_C = \frac{3}{2}$; (g-h) $I_C = \frac{-3}{2}$ and (i-j) $I_C = \frac{1}{2}$ dark C-point respectively. Left and right helicity are denoted as h_L and h_R respectively. By tracking the sign of α in equation (5), in order to make the twist of the Möbius strips more clear, one half of the major axis of the local polarization ellipse is colored blue, and the other half is colored red. Here, (a)–(h) are the examples of bright C-point, and (i)–(j) are the examples of dark C-points respectively. The projection of the polarization major axis onto a plane (xy-plane) transverse to the propagation direction z is shown at the bottom of each 3D polarization structure.

The focal plane transverse polarization distributions are shown in the bottom rows of figures 2 and 3. It can be seen that for a left-handed lemon (figure 2) the orientations of the input and the focal plane polarizations are identical. In the rectangular basis, the elipticity and handedness of polarization ellipse depends on the amplitude ratio of X and Y-components and the phase difference between these two components respectively. From column V of figure 2 it can be seen that, in the top box as indicated by red arrows, the amplitude of X-component is higher than the Y-component and thus the polarization is horizontal in this region. On the other hand, at the bottom portion, as indicated by yellow arrows, the polarization is vertical as the Y-component is higher than the X-component. At the central portion both X and Y-components have equal amplitudes and phase difference between them in $\pi/2$. Hence, the polarization is circular at the center. The handedness of focal plane transverse polarization distribution remains same as the phase difference between the X and Y-components remains constant across the entire plane.

Figure 3 shows the component amplitude and phase distributions of a right-handed lemon at the focal plane of a high numerical aperture lens. Also here, it can be seen that there is a spin–orbit coupling in the longitudinal

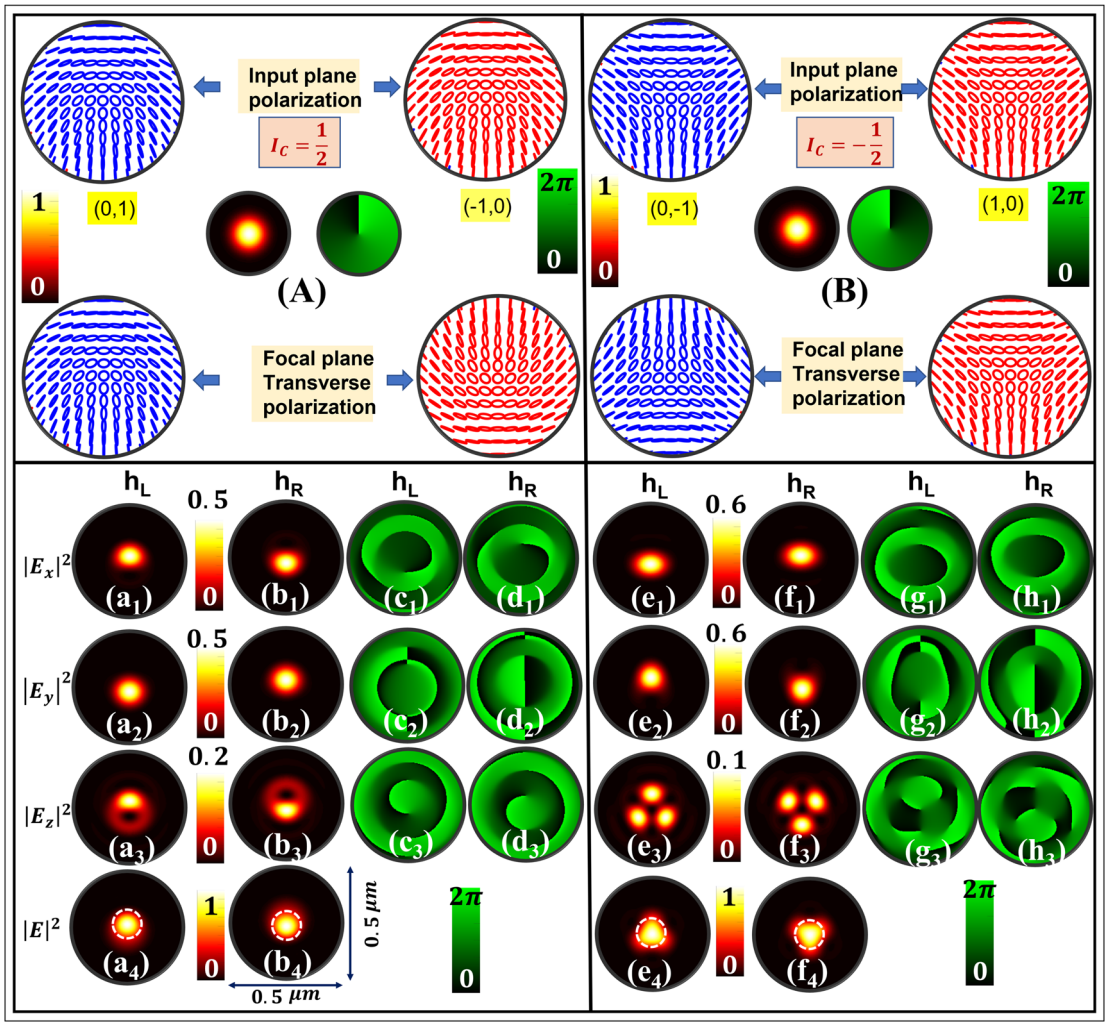

Figure 5. Bright ellipse field singularities with (A) lemon type, $I_C = \frac{1}{2}$; and (B) star type, $I_C = \frac{-1}{2}$. The top row shows the SOP, intensity, and S_{12} Stokes field phase distributions of two tightly focused beams. Focal plane transverse polarization distributions are shown as insets. The values of m and n for realizing the input C-points are given as insets. Focal plane intensities corresponding to x, y and z-components are shown in row II ($|E_x|^2$), row III ($|E_y|^2$) and row IV ($|E_z|^2$) respectively. Total intensity ($|E|^2$) distributions are shown in row V. Left and right helicity are denoted as h_L and h_R respectively. Both intensity and phase distributions corresponding to left and right helicity C-point singularity for a given C-point index are presented. Phase distributions of the field components at the focal plane are shown on the right side of the intensity distributions. Phase distributions are found to be embedded with optical vortices of charge ± 1.

component for both left-handed circularly polarized vortex beam ($m = -1$) and right-handed circularly polarized beam($n = 0$). The total longitudinal component therefore shows a spiral phase front, but in this case the winding direction is opposite to what was obtained for the left-handed lemon case. Interestingly the focal plane transverse polarization distribution undergoes 180° rotation from its initial orientation. This rotation can again be understood by inspecting the X and Y polarization components of the beam at the focal plane for a right-handed lemon. The rotation is easily observed by examining the top and bottom parts of the two field components, denoted by red and yellow arrows, in column V of figure 3. Spin-orbit coupling for the longitudinal component, as well as inversion (or lack of inversion) for the transverse polarization distribution would also occur for other C-point singularities. Specifically, the inversion of the helicity leads to 180° rotation in the focal plane intensity distribution in all the cases we will study. The transverse polarization distribution at the focal plane, as well as the intensity and phase distribution for different types of C-point singularities will be discussed in section 5.

4. Optical polarization Möbius strips

We adopt the approach introduced by M V Berry [31] to find out the 3D orientation of the polarization ellipse around the ellipse field singularity (C-point). In this representation, the major axis (α), the minor axis (β), and the normal to the polarization ellipse (Γ) in the complex representation of the electric field are described by the

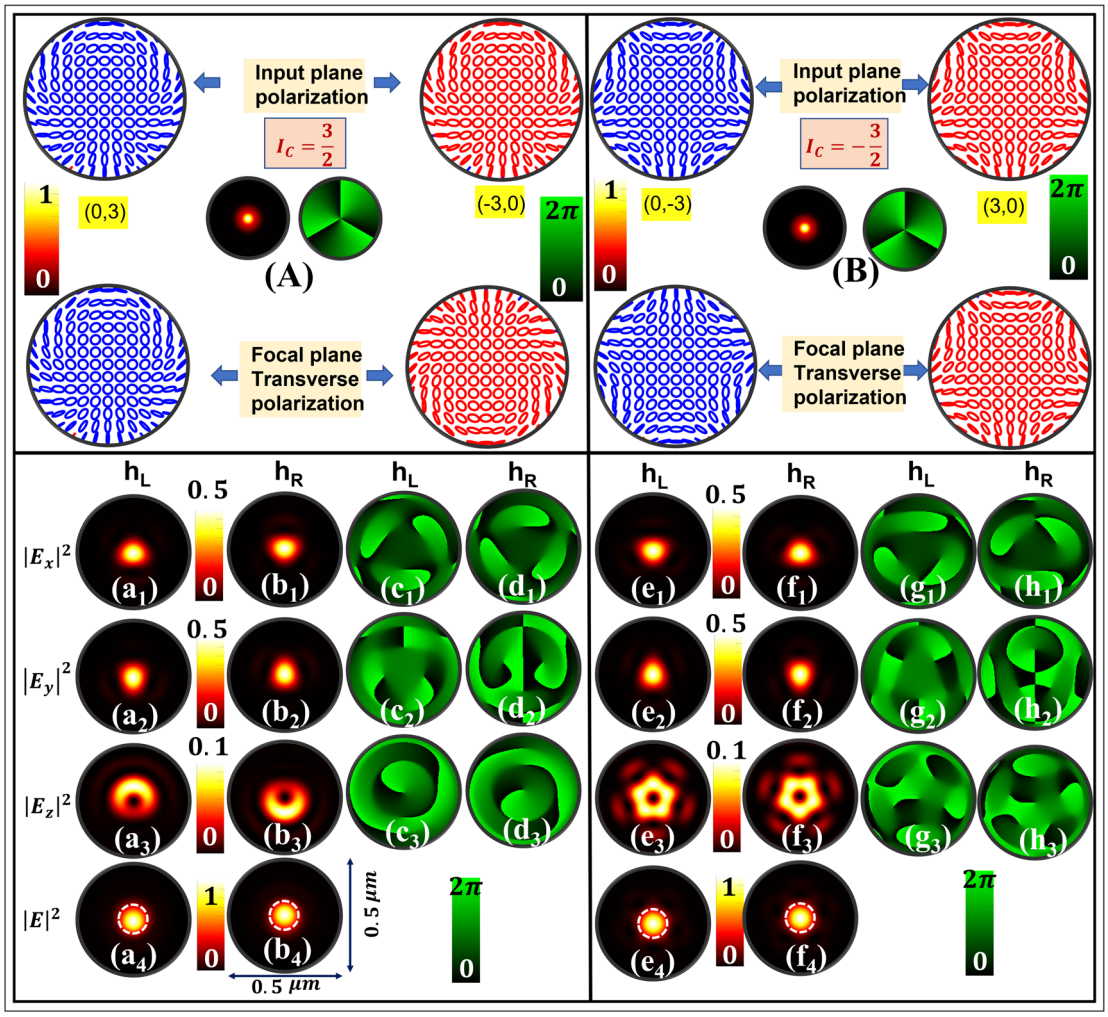

Figure 6. Bright ellipse field singularities with (A) $I_C = \frac{3}{2}$; and (B) $I_C = \frac{-3}{2}$. The top row shows the SOP, intensity, and S_{12} Stokes field phase distributions of two tightly focused beams. Focal plane transverse polarization distributions are shown as insets. The values of m and n for realizing the input C-points are given as insets. Focal plane intensities corresponding to x, y and z-components are shown in row II ($|E_x|^2$), row III ($|E_y|^2$) and row IV ($|E_z|^2$) respectively. Total intensity ($|E|^2$) distributions are shown in row V. Left and right helicity are denoted as h_L and h_R respectively. Both intensity and phase distributions corresponding to left and right helicity C-point singularity for a given C-point index are presented. Focal plane phase distributions corresponding to E_x, E_y, and E_z-component of ellipse field singularities are shown on the right side of the intensity distributions. Note that all the phase distributions are embedded with phase vortices of charge±1.

parameters as

$$\alpha = \frac{1}{|\sqrt{E \cdot E}|} Re[E^* \sqrt{E \cdot E}]$$
$$\beta = \frac{1}{|\sqrt{E \cdot E}|} Im[E^* \sqrt{E \cdot E}]$$
$$\Gamma = Im[E^* \times E], \tag{5}$$

where *Re* and *Im* denote real and imaginary parts of a complex field. E^* denotes the complex conjugate of the electric field. The sign of Γ further indicates the handedness of the polarization ellipse. In this representation, a C-line is a line in the direction of propagation, in which the major and minor axes of the ellipse become degenerate, hence the polarization becomes circular. In order to visualize and plot the polarization topology in 3D space, we considered only the polarization configuration in a plane orthogonal to the C-line, which is known as the principal plane. In particular, we considered only the focal plane, where the field's z-component is the largest. We then calculated the major and minor (α, β) axes of the polarization ellipses at all points lying on a circle in the focal plane, with a singular point (C-point) at its center. As mentioned earlier, the points at which the z- component intensity goes to zero correspond to polarization ellipses lying in the transverse plane and therefore the vector parameter Γ has vanishing x and y components. Helicity inversion of the C-point leads to handedness inversion at these specific polarization ellipse points which can be seen by the sign inversion for Γ.

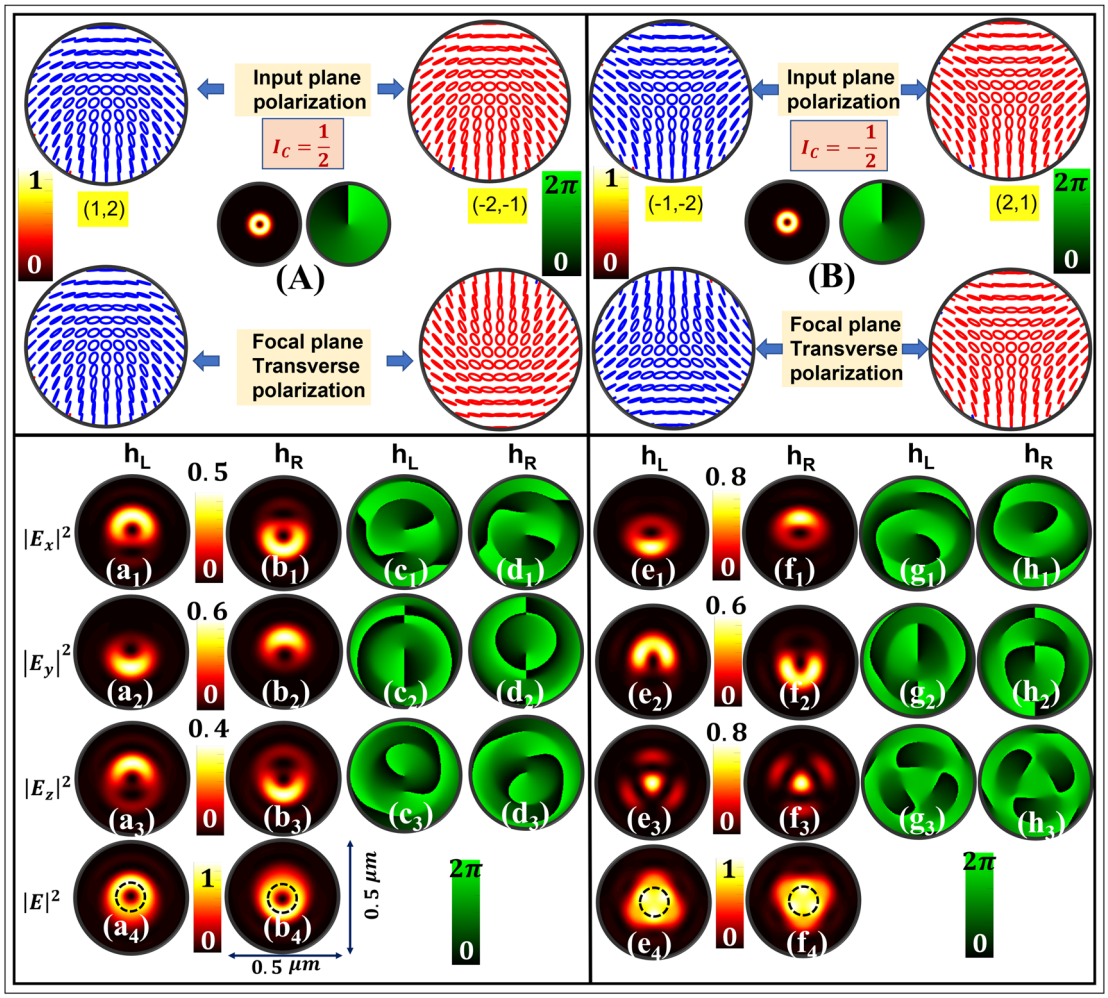

Figure 7. Nongeneric dark ellipse field singularities with (A) lemon type, $I_C = \frac{1}{2}$; and (B) star type, $I_C = \frac{-1}{2}$. The top row shows the SOP, intensity, and S_{12} Stokes field phase distributions of two tightly focused beams. Focal plane transverse polarization distributions are shown as insets. The values of m and n for realizing the input C-points are given as insets. Focal plane intensities corresponding to x, y and z-components are shown in row II ($|E_x|^2$), row III ($|E_y|^2$) and row IV ($|E_z|^2$) respectively. Total intensity ($|E|^2$) distributions are shown in row V. Left and right helicity are denoted as h_L and h_R respectively. Both intensity and phase distributions corresponding to left and right helicity C-point singularity for a given C-point index are presented. Phase distributions of the field components at the focal plane are shown on the right side of the intensity distributions. Phase distributions are found to be embedded with optical vortices of charge ± 1.

In order to numerically calculate the intensity distributions, phase distributions, and the formation of optical Möbius strips of the ellipse field singularity beams, we consider an optical system with a relatively high NA of 0.95 and an optical wavelength of 633 nm. For plotting the Möbius strips, the major axis of the 3D polarization ellipse is marked as a function of position on a circle of 200 nm radius centered on the beam axis i.e coinciding with the center of the C-point. Since a strong longitudinal component of the electric field is generated upon tight focusing, the major axis of the polarization ellipse undergoes a twist out of the focal plane in 3D space and forms a Möbius strip.

In figure 4 Möbius strips for four bright C-points (the four upper lines) and one non-generic dark C-point (the fifth line) with different polarization, singularity indices are shown and its dependence on the helicity can be clearly seen by comparing the Möbius strips in left and right column of figure 4. For a given polarization singularity index, the optical Möbius strips corresponding to left and right-handed ellipse fields are shown in the left and right columns respectively. Specifically, the Möbius strips for left and right handed bright lemon type polarization singularity, that we discussed in the previous section, are shown in figures 4(a) and (b) respectively. In table 1 number of half-twists, direction of rotations of Möbius strips, values of (m, n) and I_C values for all cases of figure 4 are presented.

It is clear from these different cases that the shape of the Möbius strips and the number of half twists depends on the helicity as well as on the sign and value of the singularity index. In figure 4 Möbius strips corresponding to $I_C = \frac{3}{2}$ has counterclockwise rotation direction, where as all other Möbius strips have clockwise rotation direction. This can be seen by fixing a symmetrical axis at a twist point [58]. By observing our results in figure 4,

we conclude that the number of half-twists for a given C-point with a C-point index (I_C) is ($|2I_C - 2|$). Moreover, if ($2I_C - 2$) is positive the rotation direction of Möbius strip is counter-clockwise and if ($2I_C - 2$) is negative the rotation direction is clockwise. It is found that the 3D polarization topology of the focal field remains unchanged but undergo a global rotation depending on the propagation distance.

5. Tight focusing and focal plane intensity distribution

In order to gain further insight, we study the intensity distribution of the different components of the electric field at the focal plane. For each input polarization distribution, the total intensity, S_{12} Stokes field phase distributions, and focal plane transverse polarization distributions are shown as insets. The circles on which the Möbius strips were plotted are shown as a dashed white or black line in the total intensity distribution of figures 5 to 7. It can be seen that in all cases the twist points correspond to zeros of the longitudinal component of the electric field. At these points, polarization ellipses lie in the transverse plane, and therefore the vector parameter Γ has vanishing x and y components as can be seen from equation (5). Helicity inversion of the C-point leads to rotation of all the component intensity distributions, as well as total intensity distribution by 180° with respect to the axial point. This is accompanied by handedness inversion at these specific polarization ellipse points which can be seen by the sign inversion for Γ. Interestingly, for a positive index right handed C-point the focal plane transverse polarization distributions undergoes 180° rotation. In case of a negative index polarization singularity the focal plane transverse polarization distributions undergoes 180° rotation only for the left handed C-point. This can be observed from figures 5–7.

Furthermore, for a bright C-point, the number of half-twists of the Möbius strips for a given input polarization distribution is the same as the number of intensity peaks present in the longitudinal component at the focal plane. The polarization distribution of positive and negative bright C-point, with index $I_C = \pm (1/2)$ and $I_C = \pm (3/2)$ are shown in figure 5 and figure 6 respectively. In both cases, the C-point is bright. The case of dark C-points with $I_C = \pm (1/2)$, is shown in figure 7. For a given C-point index, both left and right-handed C-points have the same intensity and S_{12} Stokes field phase distributions before tight focusing. The focal plane intensity corresponding to x, y, and z-component are shown in row I, row II and row III respectively. In row IV total intensity distribution at the focal plane is shown. The phase corresponding to x, y, and z-component fields are shown on the right sides. In the case of bright C-points the x, y, and z-components of the field at the focal plane are found to be embedded with phase vortices of charge ± 1. For negative polarization singularity index bright ellipse field singularities the z-component of the focal field is hosted with a central phase vortex, whereas the negative index dark ellipse field singularity does not contain any central phase singularity in the z-component of the focal plane.

Even though both bright and dark star and lemon type singularities have same polarization singularity index, the strength of longitudinal components for dark singularities are significantly higher than the corresponding generic bright C-points. In the case of bright star type singularities (figure 5(B)) there is an intensity null in the longitudinal component, whereas there is intensity maxima in the dark star type singularities (figure 7(B)). Furthermore, for dark lemon type singularities there is a central minima in the longitudinal component, which is not present in the bright lemon type singularities, as shown in figure 7(A), in comparison to figure 5(A).

6. Conclusion

In conclusion, we explored the focal plane intensity, phase, and polarization distribution of tightly focused ellipse field singularity beams. We have discussed the spin–orbit coupling and its effect on the longitudinal component of the focused beam. We have studied the formation of polarization Möbius strips, for different values of the singularity index and for opposite values of the helicity. Our work extends the family of input ellipse field singularity beams, to include the case of dark ellipse field singularities. We have also derived rules for determining the number of half-twists in polarization Möbius strips, for the case of non-integer singularity index. Our work reveals the important role of helicity in the formation of polarization Möbius strips. We show that helicity is a useful tool in shaping the focal plane amplitude and phase distributions, with potential applications in optical micromanipulation [36], material machining [39] and high-resolution microscopy [59]. The methods we discussed here can be further extended to study the focal plane amplitude distribution of Poincaré vortices [60].

Acknowledgments

The work was supported by the Israel Science Foundation, grant no. 969/22 and by Tel Aviv University Center for Light-Matter Interaction. S. K. Pal acknowledges Tel Aviv University for Pikovsky Valazzi matching scholarship. RK Singh acknowledges support by the Council of Scientific and Industrial Research (CSIR), India-Grant No 80 (0092) /20/EMR-II, and Science and Engineering Research Board (SERB) India- CORE/2019/000026.

Data availability statement

The data cannot be made publicly available upon publication because no suitable repository exists for hosting data in this field of study. The data that support the findings of this study are available upon reasonable request from the authors.

Disclosures

The authors declare no conflicts of interest.

ORCID iDs

Sushanta Kumar Pal https://orcid.org/0000-0001-5077-2373
Rakesh Kumar Singh https://orcid.org/0000-0002-3117-2695
P Senthilkumaran https://orcid.org/0000-0002-1015-0710
Ady Arie https://orcid.org/0000-0001-6486-7285

References

[1] Quabis S, Dorn R, Eberler M, Glöckl O and Leuchs G 2000 *Opt. Commun.* **179** 1–7
[2] Dorn R, Quabis S and Leuchs G 2003 *Phys. Rev. Lett.* **91** 233901
[3] Hao B, Burch J and Leger J 2008 *Appl. Opt.* **47** 2931–40
[4] Youngworth K S and Brown T G 2000 *Opt. Express* **7** 77–87
[5] Zhang W, Liu S, Li P, Jiao X and Zhao J 2013 *Opt. Express* **21** 974–83
[6] Schoonover R W and Visser T D 2006 *Opt. Express* **14** 5733–45
[7] Freund I 2005 *Opt. Commun.* **249** 7–22
[8] Bauer T, Banzer P, Karimi E, Orlov S, Rubano A, Marrucci L, Santamato E, Boyd R W and Leuchs G 2015 *Science* **347** 964–6
[9] Bauer T, Neugebauer M, Leuchs G and Banzer P 2016 *Phys. Rev. Lett.* **117** 013601
[10] Galvez E J, Dutta I, Beach K, Zeosky J J, Jones J A and Khajavi B 2017 *Sci. Rep.* **7** 13653
[11] Wan C and Zhan Q 2019 *Opt. Express* **27** 11516–24
[12] Garcia-Etxarri A 2017 *ACS Photonics* **4** 1159–64
[13] Bauer T, Banzer P, Bouchard F, Orlov S, Marrucci L, Santamato E, Boyd R W, Karimi E and Leuchs G 2019 *New J. Phys.* **21** 053020
[14] Huo P, Zhang S, Fan Q, Lu Y and Xu T 2019 *Nanoscale* **11** 10646–54
[15] Yu R, Xin Y, Zhao Q, Shao Y and Chen Y 2015 *J. Opt. Soc. Am.* A **32** 1468–73
[16] Wu L T, Guo R P, Cui T J and Chen J 2016 *J. Opt.* **19** 025101
[17] Kreismann J and Hentschel M 2018 *Europhys. Lett.* **121** 24001
[18] Xu X B, Shi L, Guo G C, Dong C H and Zou C L 2019 *Appl. Phys. Lett.* **114** 101106
[19] Freund I 2011 *Opt. Lett.* **36** 4506–8
[20] Freund I 2010 *Opt. Commun.* **283** 1–15
[21] Freund I 2010 *Opt. Commun.* **283** 16–28
[22] Freund I 2010 *Opt. Lett.* **35** 148–50
[23] Freund I 2014 *Opt. Lett.* **39** 727–30
[24] Tekce K, Otte E and Denz C 2019 *Opt. Express* **27** 29685–96
[25] Freund I 2020 *Opt. Lett.* **45** 3333–6
[26] Bliokh K Y, Alonso M A, Sugic D, Perrin M, Nori F and Brasselet E 2021 *Phys. Fluids* **33** 077122
[27] Muelas-Hurtado R D, Volke-Sepúlveda K, Ealo J L, Nori F, Alonso M A, Bliokh K Y and Brasselet E 2022 *Phys. Rev. Lett.* **129** 204301
[28] Dennis M R 2011 *Opt. Lett.* **36** 3765–7
[29] Song Y *et al* 2021 *Phys. Rev. Lett.* **127** 203901
[30] Dennis M R 2002 *Opt. Commun.* **213** 201–21
[31] Berry M V 2004 *J. Opt. A: Pure Appl. Opt.* **6** 675–8
[32] Freund I 2002 *Opt. Commun.* **201** 251–70
[33] Pal S K and Senthilkumaran P 2020 *Appl. Phys. Lett.* **117** 201101
[34] Davis J A and Nowak M D 2002 *Appl. Opt.* **41** 4835–9
[35] Samlan C T, Suna R R, Naik D N and Viswanathan N K 2018 *Appl. Phys. Lett.* **112** 031101
[36] Cipparrone G, Ricardez-Vargas I, Pagliusi P and Provenzano C 2010 *Opt. Express* **18** 6008–13
[37] Pal S K and Senthilkumaran P 2016 *Opt. Express* **24** 28008–13
[38] Pal S K, Ruchi and Senthilkumaran P 2017 *Opt. Commun.* **393** 156–68

[39] Meier M, Romano V and Feurer T 2007 *Appl. Phys.* A **86** 329–34
[40] Shen Y, Martínez E C and Rosales-Guzmán C 2022 *ACS Photonics* **9** 296–303
[41] Xu L, Zhang Y, Lang S, Wang H, Hu H, Wang J and Gong Y 2021 *J. Innov. Opt.J. Innov. Opt. Health Sci.* **14** 2050027
[42] Otte E, Tekce K and Denz C 2017 *Opt. Express* **25** 20194–201
[43] Otte E, Tekce K, Lamping S, Ravoo B J and Denz C 2019 *Nat. Commun.* **10** 4308
[44] Pal S K, Singh R K and Senthilkumaran P 2022 *J. Opt.*
[45] Cameron R P, Barnett S M and Yao A M 2012 *New J. Phys.* **14** 053050
[46] Bliokh K Y, Rodríguez-Fortuño F J, Nori F and Zayats A V 2015 *Nat. Photonics* **9** 796–808
[47] Dennis M R 2001 Topological singularities in wave fields *PhD Thesis* Bristol University
[48] Freund I, Soskin M S and Mokhun A I 2002 *Opt. Commun.* **208** 223–53
[49] Pal S K and Senthilkumaran P 2018 *Opt. Lett.* **43** 1259–62
[50] Arora G, Ruchi and Senthilkumaran P 2019 *Opt. Lett.* **44** 5638–41
[51] Richards B and Wolf E 1959 *Proceedings of the Royal Society of London A: Mathematical, Physical and Engineering Sciences* 253 358–79
[52] Singh R K, Senthilkumaran P and Singh K 2008 *J. Opt. Soc. Am.* A **25** 1307–18
[53] Zhao Y, Edgar J S, Jeffries G D M, McGloin D and Chiu D T 2007 *Phys. Rev. Lett.* **99** 073901
[54] O'Neil A T, MacVicar I, Allen L and Padgett M J 2002 *Phys. Rev. Lett.* **88** 053601
[55] Garcés-Chávez V, McGloin D, Padgett M J, Dultz W, Schmitzer H and Dholakia K 2003 *Phys. Rev. Lett.* **91** 093602
[56] Singh R K, Senthilkumaran P and Singh K 2009 *J. Opt. Soc. Am.* A **26** 576–88
[57] Ruchi Senthilkumaran P and Pal S K 2020 *International Journal of Optics* **2020** 2812803
[58] Nie Z Z, Zuo B, Wang M, Huang S, Chen X M, Liu Z Y and Yang H 2021 *Nature Commun.* **12** 1–10
[59] Hell S W and Wichmann J 1994 *Opt. Lett.* **19** 780–2
[60] Freund I 2001 *Opt. Lett.* **26** 1996–8